

Electromagnetically Actuated FR4 Scanners

Hakan Urey, *Member, IEEE*, Sven Holmstrom, and Arda D. Yalcinkaya, *Member, IEEE*

Abstract—A torsional micromechanical scanner is fabricated from thin Fire Resistant 4 substrates using standard printed circuit board technology. The top and the bottom copper layers are connected with vias and shaped as a single coil to enable one- and two-dimensional electromagnetic actuation with an external magnet. Using $5\text{ mm} \times 5\text{ mm}$ mirrors, the following scan angle and resonant frequency combinations are achieved: 17° at 1.8 kHz and 140° at 417 Hz . Another $10\times$ improvement in magnetic actuation torque seems feasible. The technology offers a unique advantage by allowing a high degree of integration with microoptics and electronics directly on the mechanical platform and offers a low-cost alternative to silicon microelectromechanical systems devices particularly when large or low-frequency devices are required.

Index Terms—Actuators, Fire Resistant 4 (FR4), optical micro-electromechanical systems (MEMS), scanners.

I. INTRODUCTION

FIRE Resistant 4 (FR4) is the most widely used material for printed circuit board (PCB). It offers good electrical, mechanical, and thermal properties. In addition to its common usage in the field of electronics, micromechanical devices can as well be fabricated with high-precision and low-cost on PCBs. FR4 has recently been adapted for board level optical interconnects that integrate microoptics and optoelectronics on PCBs [1]–[3].

In this letter, we present for the first time FR4 as a micromechanical device platform, where microoptical, mechanical, optoelectronic, electrical, and electromagnetic actuator components can be integrated on the same platform. FR4 provides fast and low-cost design and fabrication as well as a high degree of flexibility compared to conventionally used materials such as silicon microelectromechanical systems (MEMS) devices or conventional scanners [4]–[6]. The fabrication is fully realizable with standard PCB machinery. Copper coils for actuation are printed on both sides of a thin FR4 substrate, which can then be tailored into the desired device shapes by cutting. In another implementation, NiFe or other magnetic films are plated on FR4 for electromagnetic actuation with an external coil [7].

II. ELECTROMAGNETIC ACTUATOR

The Lorentz-type plastic actuator is shown in Fig. 1(a) and fabricated using standard PCB technology using $130\text{-}\mu\text{m}$ -thick

Manuscript received July 20, 2007; revised October 11, 2007. This work was supported in part by Microvision, Seattle, WA. The work of H. Urey was supported by the Turkish Academy of Sciences (TÜBA) Distinguished Scientist Award.

H. Urey and S. Holmstrom are with the Electrical Engineering Department, Koç University, TR-34450 Istanbul, Turkey (e-mail: hurey@ku.edu.tr).

A. D. Yalcinkaya is with the Electrical and Electronics Engineering Department, Boğaziçi University, TR-34342 Istanbul, Turkey.

Color versions of one or more of the figures in this letter are available online at <http://ieeexplore.ieee.org>.

Digital Object Identifier 10.1109/LPT.2007.911522

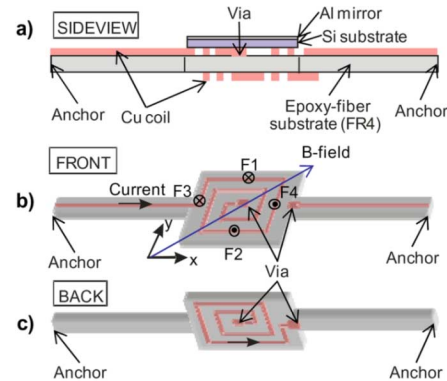


Fig. 1. Schematic drawing of the FR4 Lorentz-type electromagnetic actuator. (a) Side view of the device. (b) Front-side of the device, where 45° inclined B-field is shown. (c) Back-side of the device.

FR4 substrate with copper laminates on both sides. A $100\text{-}\mu\text{m}$ -thick mirror is diced from an Al-coated silicon wafer and bonded on top of the coil and an external permanent magnet is placed underneath the device. The device is fixed at both ends (marked as anchor) and is free to rotate about the x- and y-axis, when properly actuated. The actuation of the device is performed by the creation of Lorentz forces in the presence of a direct current (dc) magnetic field and current carrying conductors. As shown in Fig. 1(b) and (c), when an alternating current flows through the copper lines, the magnetic field will induce forces out-of-mirror plane that are lumped into four components. They are shown with their directions in Fig. 1(b). The magnitude of each force component is equal to the product of the conductor length in the current flow direction, the magnetic field normal to the current direction, and the magnitude of the current [1]. Forces F_1 and F_2 exert a net torque about the x-axis (torsion mode or slow-scan mode) and forces F_3 and F_4 exert a torque about the y-axis (out-of-plane rocking mode or fast-scan mode). There is no independent design parameter making it possible to freely choose the ratio between fast- and slow-scan.

III. LASER SCANNING

A selection of the fabricated Lorentz scanner-type actuator designs and their performances, respectively, are shown in Fig. 2 and Table I. Scanner B gives a total optical scan angle (θ_{TOSA}) of 140° at a resonance frequency of 414.2 Hz at 250 mA (corresponding to 73.75 mW). With a $5 \times 5\text{ mm}$ mirror, this gives a $\theta_{\text{TOSA}} * D$ -product of $700\text{ deg} \cdot \text{mm}$. In the rocking mode (fast-scan), a θ_{TOSA} of 10.2° at 647.3 Hz is reached for the same current. Fig. 3(a) and (b) illustrates finite-element simulations for the torsion and the rocking modes for one design. The resonance characteristics of the slow-scan mode of Scanner B, extracted at low drive current (10 mA), is given in Fig. 3(c), where the maximum θ_{TOSA} of 24.8° is obtained at 420 Hz . Certain trends were observed regarding the mechanical quality

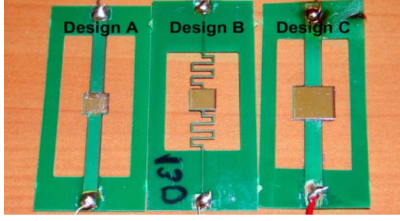


Fig. 2. Pictures of three designs of Lorentz-type actuators. Mirror dimensions for A and B are 5×5 mm and for C 8×8 mm. FR4 thickness is $130 \mu\text{m}$ and copper layer thickness on each side is $30 \mu\text{m}$.

TABLE I
SLOW SCAN PERFORMANCE FOR THE LORENTZ SCANNER DESIGNS AT LOW AND HIGH CURRENTS, RESPECTIVELY. Q IS THE QUALITY FACTOR, AND THE PRODUCT $f^2\theta_{\text{TOSA}}$ IS A FIGURE OF MERIT. MAGNETIC FLUX DENSITY IS 0.15 T

Scanner	54mA					250mA	
	Power [mW]	$f = \text{Res. Freq. [Hz]}$	$\theta_{\text{TOSA}} [\text{deg}]$	Q	$f^2\theta_{\text{TOSA}} [\text{kHz}^2\text{deg}]$	$\theta_{\text{TOSA}} [\text{deg}]$	$f^2\theta_{\text{TOSA}} [\text{kHz}^2\text{deg}]$
(A)	3,79	1787,0	4,8	38,0	15	16,9	52
(B)	3,36	417,4	83,1	49,7	14	140,0	24
(C)	9,92	807,0	10,9	26,9	7	30,0	17

(Q) factor. Q decreases with cantilever length and increases with scanner thickness. Also of interest is that scanners, such as Scanner B, that vibrate in bending mode have a considerably higher Q than those utilizing pure torsion. As can be seen in Fig. 4, the scan angle increases linearly at low drive currents, and its rate slowly drops due to spring stiffening effect at higher drive amplitudes. Two-dimensional (2-D) scans are performed using a single coil, fed with two sinusoidal signals, their frequencies corresponding to respective resonance mode. Due to relatively high mechanical Q -factors, the modes are separated. The scanner can thus be seen as a multibandpass filter for frequencies that correspond to its vibration modes [8]. At 250 mA, a 2-D scanning pattern of $66.5^\circ \times 10.2^\circ$ is obtained, as shown in Fig. 5. The torsion mode (slow-scan) can be operated off-resonance at a low frequency or even dc in one axis to achieve simpler 2-D sinusoidal raster patterns. With the single coil geometry presented, pointing applications are not possible as the fast axis has to be resonant. This limitation can be overcome by using two coils or by resorting to double-gimbal structures. Several types of mounts have been tested for the Lorentz-type actuators. To get the most rigid mounting possible, the frames of the scanner were tightly clamped between two precision machined aluminum pieces. Since this did not significantly enhance the performance, most of the tests have been performed with the scanner adhered to a 1.6-mm-thick FR4 piece, which is tailored to fit the scanners. In several vacuum tests, the pressure is lowered to below 6.6×10^{-5} atm to examine the influence of atmospheric damping. The observed increase of Q was in all cases less than 10%. These observations show together that the mechanical behavior of the scanners is dominated by the structural damping.

The fundamental resonance frequency and the mechanical actuation torque of the scanners can be written as

$$f = \frac{1}{2\pi} * \sqrt{K/I_{\text{mass}}} \quad (1)$$

$$T_{\text{mech}} = K\theta_{\text{mech}}/Q \quad (2)$$

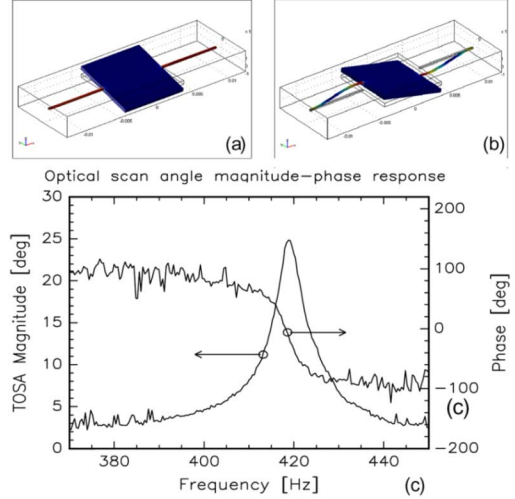


Fig. 3. Finite-element simulations of (a) the torsion (slow-scan) mode and (b) the rocking (fast-scan) mode. These modes can be generalized to all designs. (c) Magnitude and phase behavior of the slow-scan mode at low (10 mA) drive current level for Design (B). An expected a phase-shift of 180° accompanies the resonance peak.

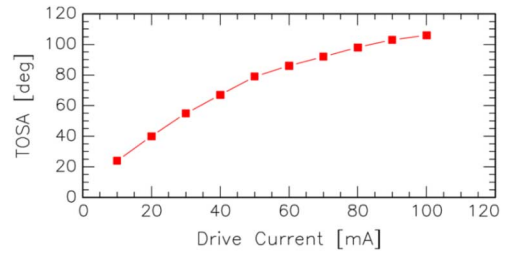


Fig. 4. Drive current—Mechanical response linearity of a $130\text{-}\mu\text{m}$ -thick Design (B) Lorentz actuator.

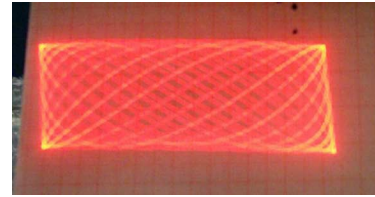


Fig. 5. Two-dimensional sinusoidal scan pattern of $66.5^\circ \times 10.2^\circ$ using Design (B).

where K is the torsional stiffness, I_{mass} the mass moment of inertia, θ_{mech} is $\theta_{\text{TOSA}}/4$ and Q is the mechanical Q -factor [9]. Setting T_{mech} equal to the magnetic actuation torque T_{mag} yields

$$f^2\theta_{\text{TOSA}} = \frac{T_{\text{mag}}Q}{\pi^2 I_{\text{mass}}} \quad (3)$$

which is introduced here as a figure of merit. Q is limited by structural damping and is in the range 30–70 for most of the tested devices. I_{mass} is mainly dependent on the design, whereas T_{mag} is determined by current, actuation coils, and the external magnetic field. Equation (3) is a good metric for comparing the performances between scanners with large differences in operation frequencies. The present scanners obtain $50 \text{ kHz}^2 \cdot \text{deg}$

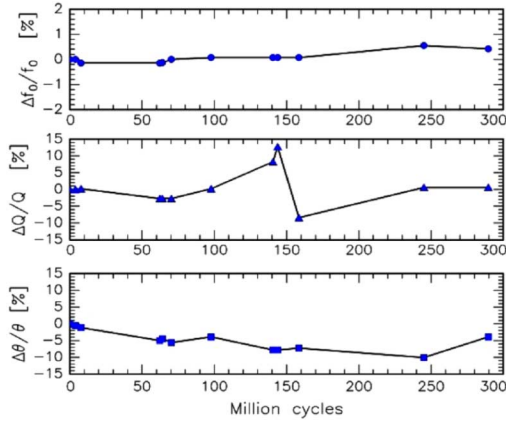


Fig. 6. Reliability test results of the Lorentz actuator. The device is kept at slow-scan resonance for about 300×10^6 cycles. Nominal values were $f = 546$ Hz, $Q = 50$, and $\theta_{\text{TOSA}} = 17^\circ$, all at 103.3 mA. The scanner used for these plots were 1.6-mm-thick FR4.

when driven at 50 mA, but there is room for improvement of this figure by a factor of 10–20. The magnetic field could be increased to 500 mT with a better magnet design. Coil current can be increased by about 50% by lowering the resistances of the vias. A ten-layer PCB is a standard process which would allow for an increase in the number of coil turns by a factor of 5. Lithographic patterning techniques could be used to write more coils in the same area. Magnetic hysteresis is not a problem in resonant mode operation and mechanical hysteresis is not observed in these structures and can generally be eliminated with engineering of the vibration mode frequencies.

The effective magnetic field during the measurements was about 150 mT. An advantage of FR4 as a scanner material is its reliability and resistance against stress and heat. Long-term reliability characteristics were tested by keeping a scanner in resonance for 288×10^6 cycles. The variation of each monitored parameter is plotted in Fig. 6. None of the scanner performance parameters exhibit a deviation of more than 10%. The maximum variation in resonance frequency was less than 1%.

Maximum relative changes in Q and scan angle are on the order of 10%, which can be explained by the changing temperature and humidity in the laboratory environment during the nearly two-week test period. Increasing current leads to successive heating of the coils. The presented designs of the Lorentz-type actuators are all stable up to currents of 250 mA. At this current, the coil [design (C)] reaches a surface temperature of 66 °C. At significantly higher currents, permanent damage may occur. At temperatures above the glass transition temperature T_g (120 °C–180 °C depending on resin chemistry) polymer reflow might occur, changing the scanner behavior. FR4 is an anisotropic material, making the modeling nontrivial. The glass fibers are intersecting only in-plane, resulting in less rigidity in out-of-plane. Also, the in-plane properties show anisotropy, but for most purposes FR4 can be modeled as transversely isotropic (see Table II) [10].

IV. CONCLUSION

FR4 and standard PCB machining techniques are used to produce low-cost, simple, and relatively high-performance me-

TABLE II

* EMPIRICAL DATA BASED ON THE LORENTZ ACTUATORS. IN A FINITE-ELEMENT MODEL ASSUMING ISOTROPY EXPERIMENTAL DATA WERE FIT TO EXPLAIN THE TORSIONAL SCANNING BEHAVIOR OF 130- μm -THICK SCANNERS, RESULTING IN THESE NUMBERS. ** MODELED DATA FROM WARNER, ASSUMES LIMITED ANISOTROPY [10]

	E [GPa]	G [GPa]	ν	CTE
Lorentz scanners*	15.0	6.25	0.2	-
In-plane**	12.8	2.57	0.13	22.8
Out-of-plane**	6.50	1.96	0.50	73.0

chanical scanners. FR4 allows for large and low-frequency devices, which is difficult to achieve with silicon MEMS.

The most important feature and a unique advantage is the large degree of integration with electronics, microoptics, and optoelectronics directly on the mechanical device platform. Other important advantages can be listed as large scan angle, low power consumption, simple design, rapid and low-cost manufacturing compared with other macro-scanners and silicon MEMS. For resonant low-frequency devices, FR4 scanners can outperform existing silicon scanners. At moderate frequencies, they constitute an inexpensive alternative to traditional material in less demanding applications [6]–[8]. A new figure of merit $f^2\theta_{\text{TOSA}}$ is introduced for assessing scanner performance. The Lorentz actuated scanner presented here achieve $50 \text{ kHz}^2 \cdot \text{deg}$ and a θ_{TOSA} D-product of $700 \text{ deg} \cdot \text{mm}$. A factor of 10–20 increase should be feasible in the $f^2\theta_{\text{TOSA}}$ metric. Tests confirmed that FR4 has good reliability for scanning applications when used in bending and torsion modes. Thus, FR4 is a good candidate for a number of optical microsystems applications.

ACKNOWLEDGMENT

The authors would like to thank Aselsan Inc., Ankara, Turkey, and Ü. Tümkaya for help with the PCB prototypes.

REFERENCES

- [1] G. v. Steenberge *et al.*, “Development of a fabrication technology for integrating low cost optical interconnects on a printed circuit board,” *Proc. SPIE, Photonics Packaging Integration VI*, vol. 6126, pp. 25–33, 2006.
- [2] H. Suyal, A. McCarthy, A. C. Walker, A. J. Waddie, and M. Taghizadeh, “Direct laser written polymer structures and passive devices for photonics applications,” in *2005 Conf. Lasers Electro-Optics Eur.*, Munich, Germany, 2005, p. 505.
- [3] P. Rabiei, W. H. Steier, Z. Cheng, and L. R. Dalton, “Polymer micro-ring filters and modulators,” *J. Lightw. Technol.*, vol. 20, no. 11, pp. 1968–1975, Nov. 2002.
- [4] H. Miyajima *et al.*, “A durable, shock-resistant electromagnetic optical scanner with polyimide-based hinges,” *J. Microelectromech. Syst.*, vol. 10, no. 3, pp. 418–424, Sep. 2001.
- [5] Y. W. Yi and C. Liu, “Magnetic actuation of hinged microstructures,” *J. Microelectromech. Syst.*, vol. 8, no. 1, pp. 10–17, Mar. 1999.
- [6] G. F. Marshall, *Optical Scanning*. New York: Marcel Dekker, 1991.
- [7] A. D. Yalcinkaya, H. Urey, and S. Holmstrom, “NiFe plated biaxial MEMS scanner for 2-D imaging,” *IEEE Photon. Technol. Lett.*, vol. 19, no. 5, pp. 330–332, Mar. 1, 2007.
- [8] A. D. Yalcinkaya, H. Urey, T. Montague, D. Brown, and R. Sprague, “Two axis electromagnetic microscanner for high resolution displays,” *IEEE J. Microelectromech. Syst.*, vol. 15, no. 4, pp. 786–794, Aug. 2006.
- [9] A. D. Yalcinkaya, O. Ergeneman, and H. Urey, “Polymer magnetic scanners for bar code applications,” *Sens. Actuators*, vol. 135, pp. 236–243, 2007.
- [10] M. Warner, J. Parry, C. Bailey, C. Marooney, H. Reeves, and K. Pericleous, “Flow/stress: An integrated stress solver for the CFD tool flowtherm,” in *Proc. IPACK’01*, Kauai, HI, Jul. 8–13, 2001, pp. 1–10, Paper 157740.